

Rigid-Body Attitude Stabilization with Attitude and Angular Rate Constraints

Qiang Shen ^a, Chengfei Yue ^b, Cher Hiang Goh ^b, Baolin Wu ^c, Danwei Wang ^d

^a Temasek Laboratories, National University of Singapore, Singapore 117411

^b Department of Electrical and Computer Engineering, National University of Singapore, Singapore 117583

^c School of Astronautics, Harbin Institute of Technology, 150080, Harbin, People's Republic of China

^d School of Electrical and Electronic Engineering, Nanyang Technological University, Singapore 639798

Abstract

In this paper, a solution to the problem of rest-to-rest three-axis attitude reorientation of a fully actuated rigid body under multiple attitude-constraint zones and angular velocity limits is presented. Based on the unit-quaternion parameterized attitude-constrained zones, a quadratic potential function is developed with a global minimum locating at the desired attitude and high potential closing to the constrained zones. In addition, to limit the magnitude of the angular velocity, another logarithmic potential function is also designed. Using these two potential functions and sliding mode control technique, a nonlinear attitude control law is obtained to guarantee asymptotic convergence of the closed-loop system with consideration of attitude and angular rate constraints, and external disturbances. The effectiveness of the constrained attitude control method is demonstrated through numerical simulation.

Key words: Rigid-body attitude control; Attitude constraint; Angular rate constraint.

1 Introduction

Rigid-body attitude control is one of the most widely studied research fields in control literature. Extensive nonlinear control algorithms have been proposed for three-axis attitude control problem of a fully actuated rigid body, such as sliding mode control [3], [20], [26], backstepping control [16], adaptive control [8], [25], hybrid control [7], and inverse optimal control [17], [21]. For the case of underactuated dynamical systems, several approaches of solving the stabilization problem have also been developed, such as [23], [10], [1], [19], just to name a few. Recently, multiple application-specific constraints in rigid-body attitude maneuver have attracted a great deal of interest. For rigid spacecraft implementations, instruments equipped on the spacecraft are re-

quired to point their boresight along a target direction while keeping away from direct exposure to sunlight or other bright objects [18]. For example, the infrared telescopes may slew from one direction to another without direct exposure to the sun vector or other infrared bright regions in space [22]. This kind of constraint is regarded as attitude constraint. Another constraint to be taken into account is angular rate constraint caused by the saturation limitation of low-rate gyro or mission specification requirement. An practical example is X-Ray Timing Explorer (XTE) spacecraft that is required to maneuver within the saturation limit of rate gyros [30]. In view of these practical considerations, this paper studies the three-axis reorientation problem of a fully actuated rigid body subject to both of attitude and angular rate constraints.

Methods dealing with attitude constrained rigid-body reorientation problem can be generalized into two main categories: path planning methods and potential function methods. In literature, several attitude path planning strategies [11], [9], [15], [6] have been developed to find the admissible rotation trajectory. However, these methods have a complex structure which gives rise to

* Corresponding author Q. Shen. Tel. +65 9426 1256. Fax +65 6872 6840.

Email addresses: tslshen@nus.edu.sg (Qiang Shen), chengfei_yue@u.nus.edu (Chengfei Yue), elegch@nus.edu.sg (Cher Hiang Goh), wubaolin@hit.edu.cn (Baolin Wu), edwwang@ntu.edu.sg (Danwei Wang).

demanding computation burden [2], [18]. Potential function methods utilize the artificial potential to model the admissible attitude path. In general, the developed artificial potential is formulated with a global attractive minimum at the desired orientation and high potential closing to the exclusion zones. Then, the potential function is incorporated in the attitude controller design to stabilize the system while satisfying attitude constraints. Since this kind of approach is analytical without changing the overall structure of the attitude control software or hardware, it is suitable for on-board computation and provides flexible autonomous operations. In [22], the potential function was formulated in the form of Gaussian functions, and an attitude controller was developed to converge the attitude without violating pre-defined pointing constraints. However, since Euler angles were used to represent attitude in [22], the proposed control algorithm may suffer from singularity. In [24], an attitude control law was synthesized applying the potential function method to prevent the camera from exposing to the Sun light directly during the slew maneuver. In [18], a convex logarithmic barrier potential was formulated in the unit-quaternion space, and the backstepping technique based controllers were proposed to ensure attitude convergence and forbidden attitude avoidance. In [27], a velocity-free attitude controller was developed for a flexible spacecraft in the presence of attitude constraints.

Another challenge in practical rigid-body attitude control is the constraint on angular rate. To ensure that angular rate is always within a pre-defined bound determined by saturation limit of rate gyros or performance requirements, several methods have been proposed. In [30], a quaternion feedback control law was developed for the near-minimum-time eigenaxis reorientation problem of the XTE spacecraft with consideration of angular velocity and control torque constraints. Although this approach is commonly used in practical spacecraft mission, a rigorous stability proof of the closed-loop system is not given. In [5], a time-efficient angular steering law was developed to handle several state constraints, where the angular rate and acceleration limits were determined by a braking curve-like angular velocity trajectory. In [12], a robust nonlinear controller incorporating a control allocation scheme was proposed for a rigid spacecraft under angular velocity constraints and actuator saturation, where a logarithmic barrier potential function was developed. In [13], an attitude stabilization strategy was proposed to solve the unwinding problem for a rigid spacecraft in the presence of angular velocity constraints.

In this paper, to handle attitude constraints and angular rate limitations simultaneously in attitude maneuver, an adaptive attitude controller based on two different potential functions defined in attitude orientation and angular velocity domain is presented. We prove that the proposed attitude controller is able to achieve asymptotic stabilization of the closed-loop system, while attitude and angular velocity constraints are satisfied concurrent-

ly. The main contributions of this study are summarized as the following three key-points:

- (1) Comparing with aforementioned literatures [18], [22], [30], [24], [27], [5], [12], [13], this study presents a solution to deal with both attitude constraints and angular rate limits in attitude control.
- (2) A logarithmic potential function in terms of sliding vector is first proposed, whose largest potential is placed at the maximal angular velocity respectively. Based on this potential function, angular velocity constraint is satisfied through limiting the magnitude of the sliding vector.
- (3) The proposed two potential functions for attitude and angular velocity are smooth and strictly convex with global minima located at the desired attitude and angular velocity. This ensures that attitude and angular velocity could be stabilized to the global minima while avoiding multiple attitude constrained zones and limiting the magnitude of angular velocity.

The remainder of this paper is organized as follows. In Section II, unit-quaternion is introduced for attitude representation, and rigid-body dynamics and modelling of attitude-constraint zones as well as angular rate limits are described. In Section III, two potential functions are designed to describe the attitude constrained zones and angular velocity limits, respectively. Then, an adaptive attitude control law using sliding mode control technique is developed to guarantee asymptotic stability. The simulation results are given in Section IV, followed by conclusions in Section V.

2 Preliminaries

In this paper, the unit-quaternion representation is used to describe the orientation of a rigid body. The set of unit quaternion \mathcal{Q}_u is given by

$$\mathcal{Q}_u = \{Q = [q^T \ q_0]^T \in \mathcal{R}^3 \times \mathcal{R} \mid q^T q + q_0^2 = 1\}. \quad (1)$$

where \mathbf{q} and q_0 denote the vector part and the scalar part of a quaternion, respectively. The unit-quaternion conjugate or inverse is defined as $Q^* = [-q^T \ q_0]^T$. The properties of quaternion can be found in [4].

2.1 Kinematics Equation

The spacecraft kinematics in terms of the unit quaternion is given by [28]

$$\dot{Q} = \frac{1}{2} Q \otimes \nu(\omega) = \frac{1}{2} \begin{bmatrix} S(\mathbf{q}) + q_0 I_3 \\ -q^T \end{bmatrix} \omega \quad (2)$$

where $\boldsymbol{\omega} \in \mathcal{R}^3$ is the inertial angular velocity vector of the spacecraft with respect to an inertial frame \mathcal{I} and expressed in the body frame \mathcal{B} , the notation “ \otimes ” denotes the quaternion multiplication operator, the function $\boldsymbol{\nu}: \mathcal{R}^3 \rightarrow \mathcal{R}^4$ is defined as the mapping $\boldsymbol{\nu}(\boldsymbol{\omega}) = [\boldsymbol{\omega}^T \ 0]^T$, and the matrix $\mathbf{S}(\boldsymbol{x}) \in \mathcal{R}^{3 \times 3}$ is a skew-symmetric matrix satisfying $\mathbf{S}(\boldsymbol{x})\boldsymbol{y} = \boldsymbol{x} \times \boldsymbol{y}$ for any vectors $\boldsymbol{x}, \boldsymbol{y} \in \mathcal{R}^3$, and “ \times ” denotes vector cross product.

Let $\mathbf{Q}_d \in \mathcal{Q}_u$ denote the desired attitude. The unit-quaternion error $\mathbf{Q}_e = [q_{e1} \ q_{e2} \ q_{e3} \ q_{e0}]^T = [q_e^T \ q_{e0}]^T \in \mathcal{Q}_u$ is given by $\mathbf{Q}_e = \mathbf{Q}_d^* \otimes \mathbf{Q} = [q_e^T \ q_{e0}]^T$. Let $\boldsymbol{\omega}_d$ denote the desired angular velocity in the desired reference frame \mathcal{N} . Since the rest-to-rest attitude maneuver is considered in this paper, the relative angular velocity defined as $\boldsymbol{\omega}_e = \boldsymbol{\omega} - \mathbf{R}(\mathbf{Q}_e)^T \boldsymbol{\omega}_d$ is simplified to $\boldsymbol{\omega}_e = \boldsymbol{\omega}$, where $\mathbf{R}(\mathbf{Q}_e)$ is \mathbf{Q}_e related rotation matrix defined as $\mathbf{R}(\mathbf{Q}_e) = (q_{e0}^2 - \mathbf{q}_e^T \mathbf{q}_e) \mathbf{I}_3 + 2\mathbf{q}_e \mathbf{q}_e^T - 2q_{e0} \mathbf{S}(\mathbf{q}_e)$ [29]. Then, the kinematics represented by unit-quaternion error is described as [28]

$$\dot{\mathbf{Q}}_e = \frac{1}{2} \mathbf{Q}_e \otimes \boldsymbol{\nu}(\boldsymbol{\omega}_e) = \frac{1}{2} \begin{bmatrix} \mathbf{S}(\mathbf{q}_e) + q_{e0} \mathbf{I}_3 \\ -\mathbf{q}_e^T \end{bmatrix} \boldsymbol{\omega}. \quad (3)$$

2.2 Rigid-Body Dynamics

The dynamics for the attitude motion of a rigid body is expressed by the following equations [29]:

$$\mathbf{J} \dot{\boldsymbol{\omega}} = -\mathbf{S}(\boldsymbol{\omega}) \mathbf{J} \boldsymbol{\omega} + \boldsymbol{\tau} + \mathbf{d} \quad (4)$$

where $\mathbf{J} \in \mathcal{R}^{3 \times 3}$ denotes the positive definite inertia matrix of a rigid body, $\boldsymbol{\tau} \in \mathcal{R}^3$ denotes the control torque about the body axes, $\mathbf{d} \in \mathcal{R}^3$ denotes the external disturbances. To design the attitude controller, a sliding vector $\mathbf{s} = [s_1, s_2, s_3]^T \in \mathcal{R}^3$ is given by

$$\mathbf{s} = \boldsymbol{\omega} + k \mathbf{q}_e \quad (5)$$

where k is a positive constant. Consequently, the attitude dynamics in terms of the sliding vector can be written as

$$\mathbf{J} \dot{\mathbf{s}} = \mathbf{f}(\boldsymbol{\omega}, \mathbf{Q}_e, \mathbf{Q}, \mathbf{s}) - k k_2 \mathbf{q}_e^T \text{Vec}[(\nabla V_a^* \otimes \mathbf{Q})] \frac{\boldsymbol{\Gamma} \mathbf{s}}{\|\mathbf{s}\|^2} + \boldsymbol{\tau} + \mathbf{d} \quad (6)$$

where the nonlinear term $\mathbf{f}(\boldsymbol{\omega}, \mathbf{Q}_e) = -\mathbf{S}(\boldsymbol{\omega}) \mathbf{J} \boldsymbol{\omega} + \frac{k}{2} (\mathbf{S}(\mathbf{q}_e) + q_{e0} \mathbf{I}_3) \boldsymbol{\omega} + k k_2 \mathbf{q}_e^T \text{Vec}[(\nabla V_a^* \otimes \mathbf{Q})] \frac{\boldsymbol{\Gamma} \mathbf{s}}{\|\mathbf{s}\|^2}$.

Assumption 1 *The external disturbance \mathbf{d} is bounded such that $\|\mathbf{d}\| \leq d_{\max}$, where d_{\max} is a positive constant and $\|\cdot\|$ denotes the Euclidean norm.*

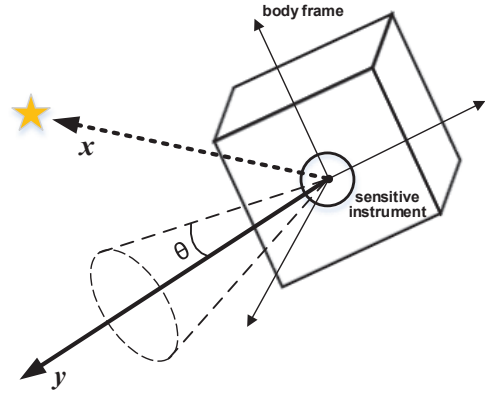


Fig. 1. Demonstration of attitude constraint.

2.3 Attitude Constraints

Suppose a half-cone angle strictly greater than θ should be maintained between the normalized boresight vector \mathbf{y} of the on-board instrument and the normalized vector \mathbf{x} pointing toward a certain unwanted object, as shown in Fig. 1. This means that the cones with an apex angle of θ emanating from the sensitive on-board instruments should exclude the unwanted objects during the reorientation maneuver. When the attitude of the rigid body is determined as \mathbf{Q} , the new boresight vector of the instrument in the inertial coordinates is expressed as

$$\begin{aligned} \mathbf{y}_I &= \mathbf{R}(\mathbf{Q})^T \mathbf{y} \\ &= (q_0^2 - \mathbf{q}^T \mathbf{q}) \mathbf{y} + 2(\mathbf{q}^T \mathbf{y}) \mathbf{q} + 2q_0 (\mathbf{q} \times \mathbf{y}) \end{aligned} \quad (7)$$

where $\mathbf{R}(\mathbf{Q})$ is a rotation matrix. Then the constraints can be expressed by the vector dot product

$$\mathbf{x} \cdot \mathbf{y}_I < \cos(\theta). \quad (8)$$

From (8), it is further obtained that

$$\mathbf{Q}^T \begin{bmatrix} \mathbf{x} \mathbf{y}^T + \mathbf{y} \mathbf{x}^T - (\mathbf{x}^T \mathbf{y}) \mathbf{I}_3 & \mathbf{y} \times \mathbf{x} \\ (\mathbf{y} \times \mathbf{x})^T & \mathbf{x}^T \mathbf{y} \end{bmatrix} \mathbf{Q} < \cos(\theta). \quad (9)$$

Suppose there are m on-board sensitive instruments equipped on the rigid body. For the j th on-board sensitive instrument, it is assumed that n constrained objectives are associated with it in the rotational space. Then, the attitude $\mathbf{Q} \in \mathcal{Q}_u$ for which the boresight vector \mathbf{y}_j with respect to the i th unwanted object should satisfy the following inequality

$$\mathbf{Q}^T \mathbf{M}_i^j \mathbf{Q} < \cos(\theta_i^j) \quad (10)$$

where

$$\mathbf{M}_i^j = \begin{bmatrix} A_i^j & b_i^j \\ b_i^{jT} & d_i^j \end{bmatrix} \quad (11)$$

with

$$\begin{aligned} A_i^j &= \mathbf{x}_i \mathbf{y}_j^T + \mathbf{y}_j \mathbf{x}_i^T - (\mathbf{x}_i^T \mathbf{y}_j) \mathbf{I}_3, b_i^j = \mathbf{y}_j \times \mathbf{x}_i, \\ d_i^j &= \mathbf{x}_i^T \mathbf{y}_j, \quad i = 1, 2, \dots, n, \quad j = 1, 2, \dots, m. \end{aligned}$$

Subsequently, a subset \mathcal{Q}_i^j of \mathcal{Q}_u that represents the possible attitude for the j th instrument with respect to the i th unwanted object, is specified as

$$\mathcal{Q}_i^j = \{\mathbf{Q} \in \mathcal{Q}_u \mid \mathbf{Q}^T \mathbf{M}_i^j \mathbf{Q} - \cos \theta_i^j < 0\}. \quad (12)$$

The angle θ_i^j is the constraint angle about the direction of the i th object specified by \mathbf{x}_i for the j th boresight vector \mathbf{y}_j . Without loss of generality, the domain of the angle θ_i^j for all i and j is restricted to be $(0, \pi)$.

2.4 Angular Rate Constraints

Due to the limited measurement range of the rate gyros or specific mission requirements, constraints on angular velocity might be required. Assuming that the angular velocity information is available, the set of angular velocity constraint is represented as

$$\mathcal{W} = \{\boldsymbol{\omega} \in \mathcal{R}^3 \mid |\omega_i| \leq \omega_{i,\max}\} \quad (13)$$

where $\omega_{i,\max}$ ($i = 1, 2, 3$) is the limitation of allowable operational angular velocity for each axis.

3 Adaptive Attitude Controller Design

In this section, two potential functions for attitude-constraint zones and angular velocity constraints are proposed, respectively. Then, an adaptive control law is designed to achieve asymptotic attitude stabilization and satisfy attitude and angular velocity constraints.

3.1 Potential Function for Attitude-Constraint Zones

The potential function $V_a(\mathbf{Q}): \mathcal{Q}_p \rightarrow \mathcal{R}$ for attitude constrained zones, is defined as [27]

$$V_a(\mathbf{Q}) = \|\mathbf{Q}_d - \mathbf{Q}\|^2 \sum_{j=1}^m \sum_{i=1}^n \frac{\alpha}{(\mathbf{Q}^T \mathbf{M}_i^j \mathbf{Q} - \cos \theta_i^j)^2} \quad (14)$$

where α is a positive constant, and the set $\mathcal{Q}_p = \{\mathbf{Q} \in \mathcal{Q}_u \mid \mathbf{Q} \in \mathcal{Q}_i^j\}$ ($i = 1, 2, \dots, n$, and $j = 1, 2, \dots, m$) represents the possible attitudes of the rigid body on which the boresight vector of the onboard instrument should lie outside of the constrained zones

Lemma 1 *The potential function in (14) has the following properties:*

- (1) $V_a(\mathbf{Q}_d) = 0$
- (2) $V_a(\mathbf{Q}) > 0$, for all $\mathbf{Q} \in \mathcal{Q}_p \setminus \{\mathbf{Q}_d\}$
- (3) $\nabla^2 V_a(\mathbf{Q}) > 0$ is positive definite for all $\mathbf{Q} \in \mathcal{Q}_p$ and $\mathbf{Q}_d \in \mathcal{Q}_p$.

Proof. See the proof of Lemma 1 in [27].

Remark 1 The proposed attitude potential function contains two parts: an attractive potential $\|\mathbf{Q}_d - \mathbf{Q}\|^2$ and a repulsive potential $\sum_{j=1}^m \sum_{i=1}^n \frac{\alpha}{(\mathbf{Q}^T \mathbf{M}_i^j \mathbf{Q} - \cos \theta_i^j)^2}$. The attractive potential measures the magnitude of the attitude error, and the repulsive potential assigns a higher artificial potential to the region around the undesired attitudes. The parameter α is used to shape the repulsive potential topology.

Remark 2 The first two properties in **Lemma 1** imply that the desired attitude \mathbf{Q}_d is the minimum of the potential function $V_a(\mathbf{Q})$. Property 3 further shows that the potential function $V_a(\mathbf{Q})$ is strictly convex for all $\mathbf{Q} \in \mathcal{Q}_p$. In light of these three properties, it is clear that the potential function $V_a(\mathbf{Q})$ has the global minimum at the desired attitude \mathbf{Q}_d . This ensures that the attitude converges to the desired value along the negative gradient of $V_a(\mathbf{Q})$ and shall not be trapped to the local minimum.

3.2 Potential Function for Angular Rate Constraints

In addition, to satisfy the angular velocity constraints, a logarithmic potential function $V_r(\mathbf{s}): \mathcal{S}_r \rightarrow \mathcal{R}$, is proposed as

$$V_r(\mathbf{s}) = \frac{1}{2} \sum_{i=1}^3 \log \left(\frac{s_{i,\max}^2}{s_{i,\max}^2 - s_i^2} \right) \quad (15)$$

where the sliding vector permissible zone \mathcal{S}_r is specified as

$$\mathcal{S}_r = \{\mathbf{s} \in \mathcal{R}^3 \mid |s_i| \leq s_{i,\max}\} \quad (16)$$

and $s_{i,\max}$ is a pre-defined maximal constant value satisfying $s_{i,\max} = \omega_{i,\max} - k > 0$ for s_i , $i = 1, 2, 3$. Meanwhile, it is assumed that $\mathbf{s}(0) \in \mathcal{S}_r$. The above logarithmic potential function is a summation of three logarithmic terms corresponding to three elements of sliding vector \mathbf{s} and guarantees that the angular velocity always stays in constrained zone defined in (13).

Lemma 2 *The potential function in (15) has the following properties:*

- (1) $V_r(0) = 0$
- (2) $V_r(\mathbf{s}) > 0$, for all $\mathbf{s} \in \mathcal{S}_r \setminus \{0\}$
- (3) $\nabla^2 V_r(\mathbf{s}) > 0$ is positive definite for all $\mathbf{s} \in \mathcal{S}_r$
- (4) If $s_{i,\max} = \omega_{i,\max} - k > 0$ for all $\mathbf{s} \in \mathcal{S}_r$, then $|\omega_i| < \omega_{i,\max}$.

Proof. See the appendix A. $\triangle \triangle \triangle$

Remark 3 Similar to **Lemma 1**, the first three properties in **Lemma 2** indicate that the potential function $V_r(\mathbf{s})$ for angular rate is smooth and strictly convex, and has the global minimum at $\mathbf{s} = 0$. The last property in **Lemma 2** shows that the angular velocity constraints can be satisfied by restricting the magnitude of the sliding vector.

3.3 Adaptive Controller Design

The adaptive attitude reorientation controller is designed as

$$\begin{aligned} \boldsymbol{\tau} = & -\boldsymbol{\Upsilon}(k_1\mathbf{s} - k_2\text{Vec}[\nabla V_a^* \otimes \mathbf{Q}]) \\ & - \mathbf{f}(\boldsymbol{\omega}, \mathbf{Q}_e, \mathbf{Q}, \mathbf{s}) - \hat{d} \frac{\boldsymbol{\Upsilon}^{-1}\mathbf{s}}{\|\boldsymbol{\Upsilon}^{-1}\mathbf{s}\|} \end{aligned} \quad (17)$$

with

$$\dot{\hat{d}} = \rho \left[\|\boldsymbol{\Upsilon}^{-1}\mathbf{s}\| - \mu(\hat{d} - \hat{d}_{max}) \right] \quad (18)$$

$$\dot{\hat{d}_{max}} = \delta(\hat{d} - \hat{d}_{max}) \quad (19)$$

where the operator $\text{Vec}[\cdot]$ denotes the vector part of $[\cdot]$, $\boldsymbol{\Upsilon} = \boldsymbol{\Psi}\mathbf{J}^{-1}$ with $\boldsymbol{\Psi} = \text{diag}\{(s_{1,\max}^2 - s_1^2), (s_{2,\max}^2 - s_2^2), (s_{3,\max}^2 - s_3^2)\}$, and the variables k_1 , k_2 , ρ , μ , and δ are positive constants. The stability of the closed-loop system with the above adaptive controller is summarized in the following theorem.

Theorem 1 *The attitude controller (17) with adaptive laws (18) and (19), applied to rigid-body attitude kinematics and dynamics expressed by (2) and (4), guarantees that all closed-loop signals are bounded and that $\lim_{t \rightarrow \infty} \mathbf{q}_e(t) = 0$ and $\lim_{t \rightarrow \infty} \boldsymbol{\omega}(t) = 0$ despite the existence of attitude-constraint zones, angular rate limits, and external disturbances.*

Proof. Consider the following Lyapunov candidate:

$$\begin{aligned} V_\ell = & 2kk_1[\mathbf{q}_e^T \mathbf{q}_e + (1 - q_0)^2] + 2k_2V_a(\mathbf{Q}) + V_r(\mathbf{s}) \\ & + \frac{1}{2\rho}(\hat{d} - d_{\max})^2 + \frac{\mu}{2\delta}(\hat{d}_{\max} - d_{\max})^2. \end{aligned} \quad (20)$$

The time derivative of V_ℓ is

$$\begin{aligned} \dot{V}_\ell = & 2kk_1\mathbf{q}_e^T \dot{\boldsymbol{\omega}} + 2k_2\nabla V_a^T \left(\frac{1}{2}\mathbf{Q} \otimes \boldsymbol{\nu}(\boldsymbol{\omega}) \right) + \mathbf{s}^T \boldsymbol{\Upsilon}^{-1} \mathbf{J} \dot{\mathbf{s}} \\ & + \frac{1}{\rho}(\hat{d} - d_{\max})\dot{\hat{d}} + \frac{\mu}{\delta}(\hat{d}_{\max} - d_{\max})\dot{\hat{d}_{\max}} \\ = & 2kk_1\boldsymbol{\omega}^T \mathbf{q}_e - k_2\boldsymbol{\omega}^T \text{Vec}[(\nabla V_a^* \otimes \mathbf{Q})] \\ & + \mathbf{s}^T \boldsymbol{\Upsilon}^{-1} \left[\mathbf{f}(\boldsymbol{\omega}, \mathbf{Q}_e, \mathbf{Q}, \mathbf{s}) + \boldsymbol{\tau} + \mathbf{d} \right. \\ & \left. - kk_2\mathbf{q}_e^T \text{Vec}[(\nabla V_a^* \otimes \mathbf{Q})] \frac{\boldsymbol{\Upsilon}\mathbf{s}}{\|\mathbf{s}\|^2} \right] \\ & + \frac{1}{\rho}(\hat{d} - d_{\max})\dot{\hat{d}} + \frac{\mu}{\delta}(\hat{d}_{\max} - d_{\max})\dot{\hat{d}_{\max}} \end{aligned} \quad (21)$$

where $\nabla V_a^T(\mathbf{Q} \otimes \boldsymbol{\nu}(\boldsymbol{\omega})) = -\boldsymbol{\omega}^T \text{Vec}[(\nabla V_a^* \otimes \mathbf{Q})]$ is used. Then, substituting the controller (17) and adaptive laws (18) and (19) in above equation, it yields

$$\begin{aligned} \dot{V}_\ell = & 2kk_1\boldsymbol{\omega}^T \mathbf{q}_e - k_1\mathbf{s}^T \mathbf{s} - \hat{d}\|\boldsymbol{\Upsilon}^{-1}\mathbf{s}\| + \mathbf{s}^T \boldsymbol{\Upsilon}^{-1} \mathbf{d} \\ & + (\hat{d} - d_{\max}) \left[\|\boldsymbol{\Upsilon}^{-1}\mathbf{s}\| - \mu(\hat{d} - \hat{d}_{max}) \right] \\ & + \mu(\hat{d}_{\max} - d_{\max})(\hat{d} - \hat{d}_{max}) \\ \leq & -k_1k^2\mathbf{q}_e^T \mathbf{q}_e - k_1\boldsymbol{\omega}^T \boldsymbol{\omega} \\ & + \mu(\hat{d} - \hat{d}_{max})(-\hat{d} + d_{max} + \hat{d}_{max} - d_{max}) \\ \leq & -k_1k^2\|\mathbf{q}_e\|^2 - k_1\|\boldsymbol{\omega}\|^2 - \mu(\hat{d} - \hat{d}_{max})^2 \leq 0. \end{aligned} \quad (22)$$

Therefore, \dot{V}_ℓ is negative semi-definite, which implies that \mathbf{q}_e , $\boldsymbol{\omega}$, $V_a(\mathbf{Q})$, $V_r(\mathbf{s})$, $\hat{d} - d_{\max}$, $\hat{d}_{\max} - d_{\max} \in L_\infty$. Since d_{\max} is a constant, it is clear that \hat{d} , $\hat{d}_{\max} \in L_\infty$. Upon integrating \dot{V}_ℓ from 0 to ∞ , one obtains

$$\begin{aligned} V_\ell(0) - V_\ell(\infty) \geq & k_1k^2 \int_0^\infty \|\mathbf{q}_e(t)\|^2 dt \\ & + k_1 \int_0^\infty \|\boldsymbol{\omega}(t)\|^2 dt + \mu \int_0^\infty (\hat{d} - \hat{d}_{max})^2 dt. \end{aligned} \quad (23)$$

It is noted that $V_\ell(0)$ is bounded because $\mathbf{Q}(0)$ and $\boldsymbol{\omega}(0)$ satisfy the attitude and angular velocity constraints. Moreover, $V_\ell(\infty)$ is also bounded as \mathbf{Q} and $\boldsymbol{\omega}$ shall be attracted to \mathbf{Q}_d and origin eventually based on properties of the two designed potential function. Therefore, the term on the left-hand side of (23) is bounded. As a result, it is clear that $\mathbf{q}_e \in L_\infty \cap L_2$, $\boldsymbol{\omega} \in L_\infty \cap L_2$, and $\hat{d} - \hat{d}_{max} \in L_\infty \cap L_2$. In addition, one can easily verify that $\dot{\mathbf{q}}_e \in L_\infty$, $\dot{\boldsymbol{\omega}} \in L_\infty$ and $\dot{\hat{d}} - \dot{\hat{d}_{max}} \in L_\infty$ from (3), (4), (18), and (19). Consequently, by invoking Barbalat's Lemma [14], it yields that

$$\lim_{t \rightarrow \infty} \mathbf{q}_e(t) = 0, \quad \lim_{t \rightarrow \infty} \boldsymbol{\omega}(t) = 0, \quad \lim_{t \rightarrow \infty} (\hat{d}(t) - \hat{d}_{max}(t)) = 0.$$

This completes the proof. $\triangle \triangle \triangle$

Remark 4 The proposed control law in (17) is discontinuous due to the last term $\frac{\mathbf{Y}^{-1}\mathbf{s}}{\|\mathbf{Y}^{-1}\mathbf{s}\|}$, which may lead to undesirable control chattering in the sliding mode. This problem can be alleviated by replacing the discontinuous function $\frac{\mathbf{Y}^{-1}\mathbf{s}}{\|\mathbf{Y}^{-1}\mathbf{s}\|}$ by a continuous function $\frac{\mathbf{Y}^{-1}\mathbf{s}}{\|\mathbf{Y}^{-1}\mathbf{s}\|+\xi}$, where ξ is a small positive scalar [31].

4 Simulation Results

To demonstrate the effectiveness and performance of the proposed controller, numerical simulation is carried out to a rigid spacecraft in this section. It is assumed that the spacecraft carries a light-sensitive instrument vector with a fixed boresight in the spacecraft body axis aligned with Z direction. The inertia matrix of spacecraft is $\mathbf{J} = \text{diag}([350, 180, 290]) \text{ kg} \cdot \text{m}^2$. The external disturbances are assumed to be

$$d = 0.001 \times \begin{bmatrix} 3 \cos(0.1t) + 4 \sin(0.03t) - 1 \\ -1.5 \sin(0.02t) - 3 \cos(0.05t) + 1.5 \\ 2 \sin(0.1t) - 1.5 \cos(0.04t) + 1 \end{bmatrix} \text{ Nm}$$

which are much larger than the real values in orbit.

Table 1
Simulation parameters

Constrained Zone (CZ)	Constrained Object	Angle
CZ 1	[0.183 -0.983 -0.036]	30 deg
CZ 2	[0 0.707 0.707]	25 deg
CZ 3	[-0.853 0.436 -0.286]	25 deg
CZ 4	[0.122 -0.140 -0.983]	20 deg

Table 2
Control parameters chosen for numerical simulation

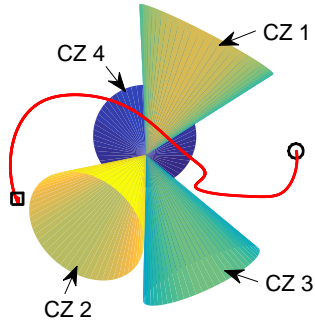
Control schemes	Control gains
Proposed controller in (17)	$\alpha = 1/30, k = 0.05, k_1 = 0.364\mathbf{J}, k_2 = 0.08\mathbf{J}, \rho = 0.01, \mu = 0.01, \delta = 0.5, \hat{d}(0) = 0.001, \hat{d}_{\max}(0) = 0.01$
Controller (58) of [18]	$k_1 = 5, \alpha = 0.364\mathbf{J}$
Controller of [30]	$k = 0.08\mathbf{J}, c = 0.364\mathbf{J}$

In the simulation, the spacecraft is retargeting its sensitive instrument while avoiding four celestial objects in the spacecraft reorientation configuration space. Four attitude-constraint zones are chosen without overlapping with each other. The details of the four attitude-constraint zones are given in Table 1, in which the normalized vectors pointing toward the corresponding celestial objects are expressed with respect to the inertial

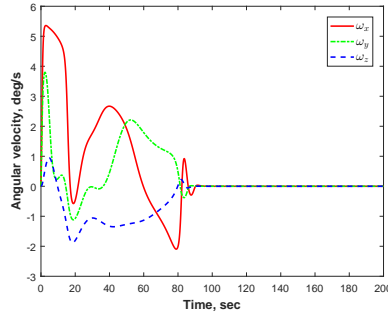
frame. The spacecraft is assumed to have the initial attitude $\mathbf{Q}(0) = [0.33 \ 0.66 \ -0.62 \ -0.2726]^T$ and initial angular velocity $\boldsymbol{\omega}(0) = [0 \ 0 \ 0]^T \text{ deg/s}$. The desired attitude that the rigid spacecraft rotates to, is selected as $\mathbf{Q}_d = [0.2 \ -0.5 \ -0.5 \ -0.6782]^T$, which locates outside of four attitude-constraint zones. Specifically, the target attitude is in a position at 30.99 deg from the center of the nearest attitude-constrained zone (i.e., CZ 2), which corresponds that the minimal angle between desired orientation and the boundary of the nearest forbidden cone is 5.99 deg. Both initial and desired attitude are chosen out of four attitude-constraint zones. The angular rate limit for each axis is assumed to be 6 deg/s. Moreover, to have a practical simulation, the limitation on the control torque is also considered to be 30 Nm. For comparison, two other attitude controllers in [18] and [30] are also simulated. The attitude controller proposed in equation (58) of reference [18] only takes attitude constraints into account, while the cascade-saturation controller in reference [30] only considers angular rate limits. The control gains for the proposed attitude controller and two others are given in Table 2.

Fig. 2a shows the trajectory of sensitive instrument pointing direction in 3D during the rest-to-rest attitude maneuver, in which four attitude-constrained zones in Table 1 are plotted inside a celestial sphere. As shown Fig. 2a, the reorientation trajectory generated by the proposed controller in (17) avoids all four constrained zones and converges the desired attitude eventually. From Fig. 2b, the angular velocity converges to a small neighbourhood of origin, and the angular velocity constraint is ensured during the attitude maneuver. The commanded control torque under the proposed controller (17) is shown in Fig. 2c.

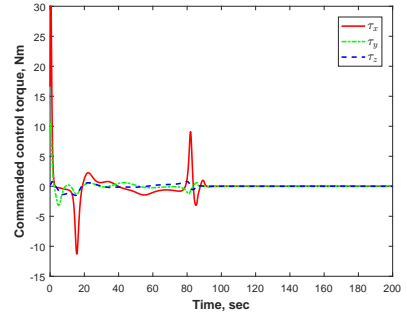
Simulation results for the attitude controllers in references [18] and [30] are given in Fig. 3. As shown in Figs. 3a and 3b, the attitude controller in reference [18] avoids all four attitude-constraint zone but the angular rate reaches to 8.37 deg/s, which exceeds the allowed maximal angular velocity. The cascade-saturation controller in reference [30] guarantees that angular velocity is always within the rate limit as depicted in Fig. 3c, but the attitude trajectory goes into the attitude-constraint zone (see Fig. 3a), which may cause damage to onboard sensitive instruments and should be avoided in attitude controller design. The quantitative analysis of these three controllers is listed in Table 3. Due to the fact that the proposed controller not only avoids all the four attitude-constraint zones but also limits the angular rate, its settling time is longer than that of the other two existing controllers that cannot handle attitude and angular velocity constraints simultaneously. Since the proposed controller is also robust to external disturbances, the steady-state errors under the proposed controller are better than the other two methods. From energy consumption perspective, the proposed controller and controller (58) of reference [18] expend much more energy



(a) Trajectory in 3D

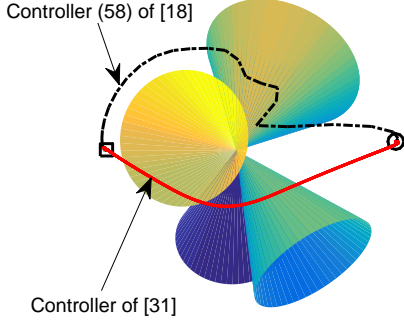


(b) Angular velocity ω

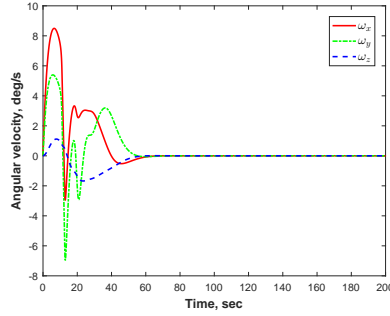


(c) Control torque τ

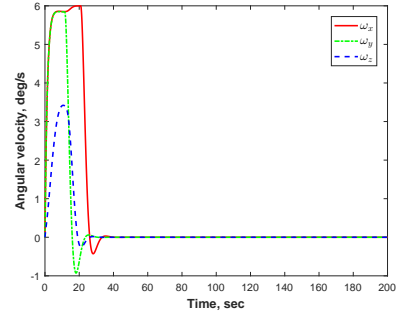
n three-dimension (3D) under the proposed control law in (17) itation are marked by “circle” and “square”, respectively. Time τ under the proposed controller are shown in (b) and (c).



(a) Trajectory in 3D



(b) Angular velocity ω under controller (58) of [18]



(c) Angular velocity ω under controller of [30]

Fig. 3. Trajectories of sensitive instrument pointing direction in 3D under the controller (58) of reference [18] and cascade-saturation controller of reference [30] are shown in (a). Time responses of angular velocity ω under the two comparative controllers of reference [18] and reference [30] are shown in (b) and (c), respectively.

Table 3
Comparison of control performance

Controller	Control performance				
	ST ¹ of q_e	ST of ω	SE ² of q_e	SE of ω	OCF ³
Proposed controller in (17)	88.9	89.6	$\pm 1.9 \times 10^{-4}$	$\pm 3.2 \times 10^{-3}$	670.73
Controller (58) of [18]	64.4	64.8	$\pm 3.1 \times 10^{-3}$	$\pm 1.5 \times 10^{-2}$	687.49
Controller of [30]	33.6	31.7	$\pm 4.8 \times 10^{-4}$	$\pm 2.0 \times 10^{-3}$	563.40

¹ ST stands for settling time in second with $|q_{e,i}| \leq 0.001$ and $|\omega_i| \leq 0.1$.

² SE stands for steady error in deg/s.

³ OCF denotes overall control effort defined as $OCF = \frac{1}{2} \int_0^T \|\tau\|^2 dt$, where T is the simulation time.

than cascade-PD controller of reference [30]. This is because extra control efforts are spent for additional attitude trajectory avoiding the attitude forbidden zones.

5 Conclusions

This paper addresses the problem of constrained attitude controller design for a rigid body in the presence of attitude-constraint zones, angular rate limits, and external disturbances. By building attitude constraints in

unit-quaternion space, a quadratic potential function that is sufficient to bring the attitude to the desired value while avoiding multiple attitude-constraint zones is proposed. In addition, to ensure that the specified maximum angular rate is not exceeded, a logarithmic potential function is also developed. Based on these two potential functions, an adaptive attitude control law is synthesized to achieve asymptotic stability of the overall closed-loop system. Numerical simulation examples are provided to show the efficiency and performance im-

provements of proposed method comparing to two existing attitude controllers that do not account for attitude and angular velocity constraints simultaneously. In future work, the control input saturation caused by actuator physical limitation should be studied to reduce the energy consumption.

Appendix

A Proof of Lemma 2

From the definition of the logarithmic potential function $V_r(\mathbf{s})$, it is clear that $V_r(0) = 0$. Moreover, for all $\mathbf{s} \in \mathcal{S}_r \setminus \{0\}$, the inequalities

$$\frac{s_{i,\max}^2}{s_{i,\max}^2 - s_i^2} > 1 \quad (\text{A.1})$$

hold, which subsequently leads to

$$\log\left(\frac{s_{i,\max}^2}{s_{i,\max}^2 - s_i^2}\right) > 0. \quad (\text{A.2})$$

Hence, $V_r(\mathbf{s}) > 0$, for all $\mathbf{s} \in \mathcal{S}_r \setminus \{0\}$.

The third part of **Lemma 2** can be obtained by taking the second order partial derivative of $V_r(\mathbf{s})$ with respect to \mathbf{s} . Since the potential function $V_r(\mathbf{s})$ is a linear combination of three logarithmic functions, it is sufficient to analyze one of the terms in more details, for example,

$$V_{ri}(s_i) = \frac{1}{2} \log\left(\frac{s_{i,\max}^2}{s_{i,\max}^2 - s_i^2}\right). \quad (\text{A.3})$$

The gradient of $V_{ri}(s_i)$ is calculated as

$$\nabla V_{ri}(s_i) = \frac{s_i}{s_{i,\max}^2 - s_i^2}. \quad (\text{A.4})$$

Consequently, the Hessian $\nabla^2 V_{ri}(s_i)$ is given as

$$\nabla^2 V_{ri}(s_i) = \frac{s_{i,\max}^2 + s_i^2}{(s_{i,\max}^2 - s_i^2)^2}, \quad (\text{A.5})$$

which implies that $\nabla^2 V_r(s_i) > 0$. Therefore, it is clear that $\nabla^2 V_r(\mathbf{s}) > 0$ if $\mathbf{s} \in \mathcal{S}_r$.

Regarding to the last property in **Lemma 2**, on the one hand, since $\mathbf{s} \in \mathcal{S}_r$ ensures $|s_i| \leq s_{i,\max}$, it is found that $\omega_{i,\max} - k \geq |s_i|$. On the other hand, in view of sliding vector in (5) and the unit-quaternion property that $|q_{ei}| \leq 1$, it is clear that $|s_i| \geq |\omega_i| - k$. Therefore, combining these two aspects, it can be obtained that $|\omega_i| \leq \omega_{i,\max}$. $\triangle \triangle \triangle$

References

- [1] G. Avanzini, E. L. de Angelis, and F. Giuliatti. Spin-axis pointing of a magnetically actuated spacecraft. *Acta Astronautica*, 94(1):493–501, 2014.
- [2] G. Avanzini, G. Radice, and I. Ali. Potential approach for constrained autonomous manoeuvres of a spacecraft equipped with a cluster of control moment gyroscopes. *Proceedings of the Institution of Mechanical Engineers, Part G: Journal of Aerospace Engineering*, 223(3):285–296, 2009.
- [3] J. D. Boskovic, S. Li, and R. K. Mehra. Robust adaptive variable structure control of spacecraft under control input saturation. *Journal Guidance, Control, and Dynamics*, 24(1):14–22, 2001.
- [4] J. K. C. Chou. Quaternion kinematic and dynamic differential equations. *IEEE Transactions on Robotics and Automation*, 8(1):53–64, 1992.
- [5] Verbin D., Lappas V. J., and J. Z. Ben-Asher. Time-efficient angular steering laws for rigid satellites. *Journal of Guidance, Control, and Dynamics*, 34(3):878–892, 2011.
- [6] E. L. de Angelis, F. Giuliatti, and G. Avanzini. Single-axis pointing of underactuated spacecraft in the presence of path constraints. *Journal Guidance, Control, and Dynamics*, 38(1):143–147, 2015.
- [7] E. L. de Angelis, F. Giuliatti, A. H. J. de Ruiter, and G. Avanzini. Spacecraft attitude control using magnetic and mechanical actuation. *Journal Guidance, Control, and Dynamics*, 39(3):564–573, 2016.
- [8] S. di Gennaro. Output stabilization of flexible spacecraft with active vibration suppression. *IEEE Transactions on Aerospace and Electronic Systems*, 39(3):747–759, 2003.
- [9] E. Frazzoli, M. A. Dahleh, E. Feron, and R. P. Kornfeld. A randomized attitude slew planning algorithm for autonomous spacecraft. In *AIAA Guidance, Navigation, and Control Conference and Exhibit*, pages 1–8, Montreal, Canada, 2001. AIAA.
- [10] D. Gasagrandea, A. Astolfi, and T. Parisini. Global asymptotic stabilization of the attitude and the angular rates of an underactuated non-symmetric rigid body. *Automatica*, 44(7):1781–1789, 2008.
- [11] H. B. Hablani. Attitude commands avoiding bright objects and maintaining communication with ground station. *Journal of Guidance, Control, and Dynamics*, 22(6):759–767, 1999.
- [12] Q. L. Hu, B. Li, and Y. M. Zhang. Robust attitude control design for spacecraft under assigned velocity and control constraints. *ISA Transactions*, 52(4):480–493, 2016.
- [13] Q. L. Hu, L. Li, and M. I. Friswell. Spacecraft anti-unwinding attitude control with actuator nonlinearities and velocity limit. *Journal of Guidance, Control, and Dynamics*, 38(10):2042–2049, 2015.
- [14] H. K. Khalil. *Nonlinear Systems*. Prentice-Hall, Upper Saddle, River, NJ, 3rd edition, 2002.
- [15] H. C. Kjellberg and E. G. Lightsey. Discretized constrained attitude pathfinding and control for satellites. *Journal of Guidance, Control, and Dynamics*, 36(5):1301–1309, 2013.
- [16] R. Kristiansen, P. J. Nicklasson, and J. T. Gravdahl. Spacecraft coordination control in 6DOF: Integrator backstepping vs passivity-based control. *Automatica*, 44(11):2896–2901, 2008.
- [17] M. Krstic and P. Tsiotras. Inverse optimal stabilization of a rigid spacecraft. *IEEE Transactions on Automatic Control*, 44(5):1042–1049, 1999.

- [18] U. Lee and M. Mesbahi. Feedback control for spacecraft reorientation under attitude constraints via convex potentials. *IEEE Transactions on Aerospace and Electronic Systems*, 50(4):2578–2592, 2014.
- [19] H. Li, W. Yan, and Y. Shi. Continuous-time model predictive control of under-actuated spacecraft with bounded control torques. *Automatica*, 75:144–153, Jan. 2017.
- [20] K. Lu and Y. Xia. Adaptive attitude tracking control for rigid spacecraft with finite-time convergence. *Automatica*, 49(12):3591–3599, 2014.
- [21] W. Luo, Y. Chu, and K. Ling. Inverse optimal adaptive control for attitude tracking of spacecraft. *IEEE Transactions on Automatic Control*, 50(11):1639–1654, 2005.
- [22] C. R. McInnes. Large angle slew maneuvers with autonomous sun vector avoidance. *Journal of Guidance, Control, and Dynamics*, 17(4):875–877, 1994.
- [23] P. Morin and C. Samson. Time-varying exponential stabilization of a rigid spacecraft with two control torques. *IEEE Transactions on Automatic Control*, 42(4):528–534, 1997.
- [24] W. Rafal and K. Piotr. Slew maneuver control for spacecraft equipped with star camera and reaction wheels. *Control Engineering Practice*, 13(3):349–356, 2005.
- [25] Q. Shen, D. W. Wang, S. Q. Zhu, and E. K. Poh. Inertia-free fault-tolerant spacecraft attitude tracking using control allocation. *Automatica*, 62:114–121, 2015.
- [26] Q. Shen, D. W. Wang, S. Q. Zhu, and E. K. Poh. Integral-type sliding mode fault-tolerant control for attitude stabilization of spacecraft. *IEEE Transactions on Control Systems Technology*, 23(3):1131–1138, 2015.
- [27] Q. Shen, C. F. Yue, and C. H. Goh. Velocity-free attitude reorientation of a flexible spacecraft with attitude constraints. *Journal Guidance, Control, and Dynamics*, 40(5):1293–1299, May 2017.
- [28] M. D Shuster. A survey of attitude representation. *Journal of the Astronautical Sciences*, 41(4):439–517, 1993.
- [29] M. J. Sidi. *Spacecraft Dynamics and Control*. Cambridge, NY: Cambridge University Press, 1997.
- [30] B. Wie and Jianbo Lu. Feedback control logic for spacecraft eigenaxis rotations under slew rate and control constraints. *Journal of Guidance, Control, and Dynamics*, 18(6):1372–1379, 1995.
- [31] X. H. Yu and O. Kaynak. Sliding-mode control with soft computing: a survey. *IEEE Transactions on Industrial Electronics*, 56(9):3275–3285, Sep. 2009.